CATALYSIS

Disentangling the activity-selectivity trade-off in catalytic conversion of syngas to light olefins

Feng Jiao[1,2]†, Bing Bai[1,2]†, Gen Li[1,2]†, Xiulian Pan[1,2]*, Yihan Ye[1,2], Shengcheng Qu[1], Changqi Xu[1], Jianping Xiao[1,2], Zhenghao Jia[1], Wei Liu[1], Tao Peng[1,3], Yilun Ding[1,2], Cheng Liu[1,2], Jinjing Li[1], Xinhe Bao[1,2,3]*

Breaking the trade-off between activity and selectivity has been a long-standing challenge in the field of catalysis. We demonstrate the importance of disentangling the target reaction from the secondary reactions for the case of direct syngas conversion to light olefins by incorporating germanium-substituted AlPO-18 within the framework of the metal oxide–zeolite (OXZEO) catalyst concept. The attenuated strength of the catalytically active Brønsted acid sites allows enhancing the targeted carbon-carbon coupling of ketene intermediates to form olefins by increasing the active site density while inhibiting secondary reactions that consume the olefins. Thus, a light-olefins selectivity of 83% among hydrocarbons and carbon monoxide conversion of 85% were obtained simultaneously, leading to an unprecedented light-olefins yield of 48% versus current reported light-olefins yields of ≤27%.

Achieving both high activity and high selectivity is a long-standing challenge for selective reactions such as the hydrogenation of CO in direct syngas conversion (*1*–*8*). Fischer-Tropsch synthesis (FTS), as a key process for syngas conversion using Fe-based (*8*–*10*) and Co-based (*11*–*13*) catalysts, allows direct synthesis of light olefins (two to four carbon atoms, $C_2^=$–$C_4^=$), named as Fischer-Tropsch-to-olefins (FTTO). Substantial progress has been made in the past decade (table S1). For example, a 61% light-olefins selectivity among hydrocarbons at 0.5 to 1% CO conversion and 52% selectivity at 88% CO conversion had been obtained, giving 26% yield of light olefins over Fe/carbon nanofiber catalysts (*8*). Hydrophobically modified FeMn catalysts gave 63% selectivity for all olefins and ~27% for light olefins at 56% CO conversion, amounting to ~14% yield of light olefins (*9*). A light-olefins selectivity of 61% among hydrocarbons was achieved at 32% CO conversion over Mn-promoted Co_2C catalysts, giving 10% $C_2^=$–$C_4^=$ yield (*11*). More recently, CO conversion was enhanced to 64%, with 71% light-olefins selectivity among hydrocarbons when CoMn carbide was physically mixed with hydrophobic polydivinylbenzene, giving 24% yield of light olefins (*13*).

In addition, bifunctional metal oxide–zeolite (OXZEO) catalysts were recently developed for direct syngas conversion to light olefins (*6*, *7*, *14*–*16*). By separating the key steps of CO and H_2 activation from the subsequent C–C coupling of the ketene intermediates (CH_2CO, which is a carrier of CH_2) on the active sites of metal oxides and zeolites (or zeotypes), respectively, the product selectivity can be modulated through the topology of zeolites (or zeotypes), and light-olefins selectivity higher than 80% was obtained (*6*, *7*, *16*). Recently, the technology was successfully demonstrated in a pilot plant with 1000 ton/year light-olefins output in Shaanxi, China (*7*, *17*). Extensive efforts have been made to optimize the catalyst by screening a wide range of metal oxide and zeolite (zeotype) combinations as well as reaction conditions (*7*, *16*, *18*–*24*). As a result, the catalytic performance has been greatly improved; CO conversion could be increased from 17 to 60% with light-olefins selectivity being maintained at 75%, and the yield of light olefins improved from 8 to 27% (*16*, *21*, *24*). However, further improvement of OXZEO and FTTO processes appears to be stalled by an activity-selectivity trade-off (Fig. 1A, dashed line, and table S1).

The mechanistic origin of the activity-selectivity trade-off can be traced to the catalytic sites for both the target and side reactions on the catalyst. Taking the silicoaluminophosphate (SAPO)–type zeotypes in the OXZEO syngas conversion concept as an example, the Si–OH–Al Brønsted acid sites are the active sites, catalyzing C–C coupling of the ketene intermediates to form light olefins as products (*7*, *18*), which consequently shifts the thermodynamically limited step of syngas conversion to ketene (*7*, *25*). A high selectivity of light olefins has been achieved by weakening the acidity through reduction of the Si content (*7*, *16*, *18*). However, this reduces simultaneously the density of the Si–OH–Al acid sites and hence the rate of intermediate consumption and ultimately CO conversion. CO conversion can be facilitated with a higher acid site density by increasing the Si content of the SAPO zeotypes. But this comes at the expense of olefins selectivity because the Si–OH–Al Brønsted acid sites are

[1]State Key Laboratory of Catalysis, 2011-Collaborative Innovation Center of Chemistry for Energy Materials, Dalian Institute of Chemical Physics, Chinese Academy of Sciences, Dalian 116023, China. [2]University of Chinese Academy of Sciences, Beijing 100049, China. [3]University of Science and Technology of China, Hefei 230026, China.
*Corresponding author. Email: panxl@dicp.ac.cn (X.P.); xhbao@dicp.ac.cn (X.B.)
†These authors contributed equally to this work.

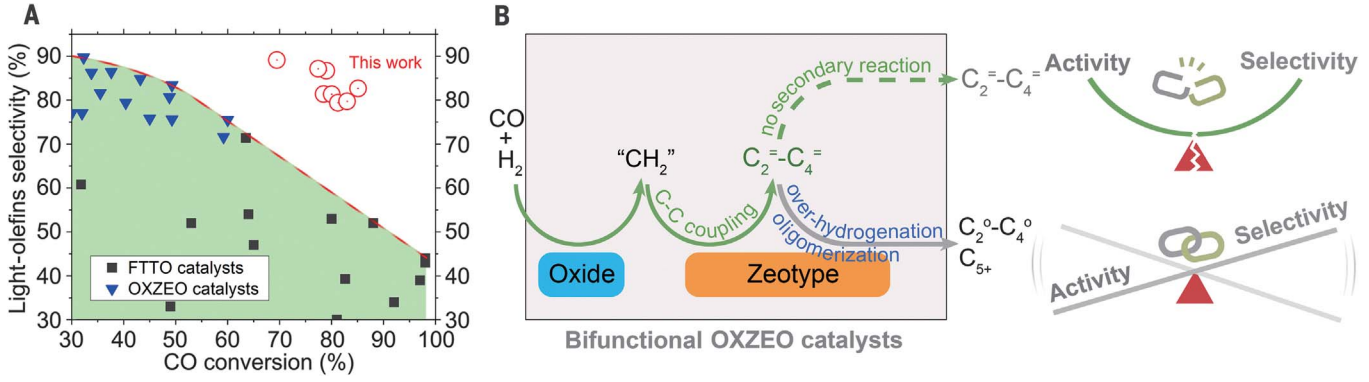

Fig. 1. The activity-selectivity trade-off in the OXZEO syngas-to-light olefins process. (**A**) Selectivity of light olefins versus CO conversion data reported for FTTO (black squares) and OXZEO (blue triangles) processes (*6*–*14*, *16*, *18*–*24*, *30*), and this work (red circles). The red dashed line is a guide for the eye. (**B**) Scheme depicting the activity-selectivity trade-off caused by the entangled target (ketene intermediate-to-light olefins) and undesired secondary reactions (overhydrogenation to paraffins and oligomerization to C_{5+} hydrocarbons) over zeotypes.

also active for the secondary reactions of olefins, such as hydrogenation and oligomerization (*18*, *26*–*28*). Moreover, these secondary reactions are enhanced by the simultaneously strengthened acidity and increased active sites (*6*, *7*, *14*, *16*, *18*, *29*). For example, Li *et al.* showed that CO conversion was enhanced from 27 to 50% by increasing the Si content of SAPO-18, but the light-olefins selectivity declined from more than 80% to around 50% because of the simultaneous acceleration of secondary hydrogenation reactions (*18*). It remains a mechanistic challenge for conventional aluminosilicate and SAPO zeotypes.

Therefore, the goal is to terminate the reaction at the olefin formation step—that is, to disentangle the target reaction C–C coupling of ketene from the secondary reactions of hydrogenation and oligomerization of olefins (Fig. 1B). We report that Ge-substituted AlPO-18 is an effective strategy to achieve this goal and thus break the activity-selectivity trade-off. As a result, we obtained an unprecedented CO conversion of 85% simultaneously with 83% light-olefins selectivity among hydrocarbons. The light-olefins yield reaches as high as 48%, which nearly doubles the best values reported previously for FTTO and OXZEO processes.

Germanium incorporation in AlPO-18

We introduced Ge into AlPO-18 by means of a hydrothermal method, with the Ge/Al ratio varying between 0.012 and 0.027 (denoted as the subscript "a"). The resulting GeAPO-18$_a$ zeotypes exhibited a typical AEI crystal structure with no impurity phase and homogenous distribution of Ge species throughout the crystals (figs. S1 to S4 and table S2). Taking GeAPO-18$_{0.025}$, for example, x-ray absorption spectroscopy (XAS) of the Ge K-edge (fig. S5 and table S3) indicated that Ge species were dispersed as single sites being fourfold coordinated with O atoms within the AlPO-18 framework. Infrared analysis of the hydroxyl (OH) stretching vibration (fig. S6) and NH_3 adsorbed on GeAPO-18$_a$ (fig. S7) confirmed the generation of Ge–OH–Al Brønsted acid sites created by the framework substitution of P by Ge atoms (figs. S8 and S9). A hydrothermal treatment experiment at 450°C demonstrated a good stability (fig. S10). NH_3 temperature-programmed desorption (TPD) indicated that the acid site density increased with the Ge/Al ratio up to 0.027, but the acid strength remained about the same (fig. S11 and table S4).

The GeAPO-18$_a$ variants were physically mixed with $ZnCrO_x$ to form OXZEO composite catalysts for syngas conversion. CO conversion reached 60% upon introduction of a small amount of Ge (Ge/Al = 0.012), and light-olefins selectivity among hydrocarbons was 84% at 410°C. CO conversion rose almost linearly to 79%, with the density of the medium-strength acid sites increasing to 53 μmol/g,

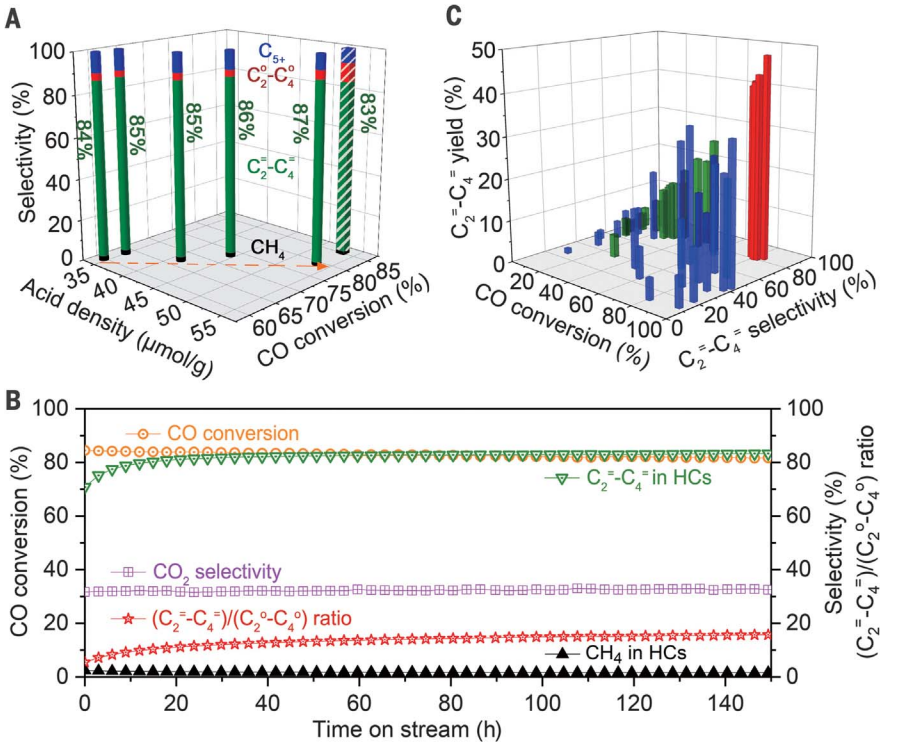

Fig. 2. Catalytic performance of $ZnCrO_x$–GeAPO-18 catalysts in syngas conversion. (**A**) Performance as a function of the medium-strength Brønsted acid site density of GeAPO-18. The dashed arrow line is a guide for the eye. Reaction condition: $ZnCrO_x$/GeAPO-18 = 2 (mass ratio), H_2/CO = 2.5, 410° and 430°C (prism filled pattern), 6 MPa and 1500 ml/(g_{cat}·hour). (**B**) Stability test of $ZnCrO_x$–GeAPO-18$_{0.027}$ at 430°C. (**C**) Performance of $ZnCrO_x$–GeAPO-18 (red columns) in comparison with previously reported FTTO (blue) and OXZEO catalysts (green) (*6*–*14*, *16*, *18*–*24*, *30*).

and light-olefins selectivity increased to 87% (Fig. 2A). CO conversion further increased to 85% at 430°C, and light-olefins selectivity declined only slightly to 83% (Fig. 2A and fig. S12). By contrast, AlPO-18 containing no Ge exhibited a low CO conversion of 24% and light-olefins selectivity of 63% under the same conditions (fig. S13 and table S5).

A test of 150 hours on stream showed that the catalyst delivered stable performance during this time frame (Fig. 2B, fig. S14, and table S6). The ratio of light-olefins to light-paraffins, denoted as $(C_2^=$–$C_4^=)/(C_2^o$–$C_4^o)$, remained at 16. The yield of light olefins reached as high as 48% (Fig. 2C), surpassing the previously reported best values for both FTTO and OXZEO catalysts by nearly a factor of 2 (*6*–*14*, *16*, *18*–*24*, *30*). The above results indicated that the "performance ceiling" shown in Fig. 1A is successfully broken, with CO conversion and light-olefins selectivity both exceeding 80%.

Catalyst comparison

To further illustrate the versatility of GeAPO-18 zeotypes, we compared them with corresponding catalysts substituted with silicon (SAPO-18) and with magnesium (MgAPO-18). Those two zeotypes were prepared with similar methods as that used for GeAPO-18 (supplementary materials) with a Si/Al ratio ranging from 0.011 to 0.029 and Mg/P ratio from 0.019 to 0.029, respectively. The resulting $ZnCrO_x$–MeAPO-18$_a$ combinations were all tested in a wide temperature range of 410° to 480°C and space velocity between 1500 to 6000 ml/(g_{cat}·hour). The CO_2 selectivity appeared to be controlled thermodynamically (figs. S15 and S16). The red-orange-yellow region of the contour plots in Fig. 3, A to C, indicates light-olefins selectivity >80%, and black regions indicate selectivity <60%. The maps indicate that GeAPO-18 allowed the reaction to be operated over a wider temperature range, in which light-olefins selectivity and CO conversion simultaneously remained >80% with the $(C_2^=$–$C_4^=)/(C_2^o$–$C_4^o)$ ratio > 15 (Fig. 3A and fig. S17). A wider operation temperature range is highly desirable for applications. By contrast, the red-orange-yellow operation zone was much smaller with the classical SAPO-18 zeotypes (Fig. 3B) and almost nonexistent with MgAPO-18 (Fig. 3C). All SAPO-18$_a$, MgAPO-18$_a$, and GeAPO-18$_a$ samples examined under different conditions in this work are detailed in Fig. 3D. It reveals that the activity-selectivity trade-off boundary cannot be exceeded with SAPO-18 and MgAPO-18

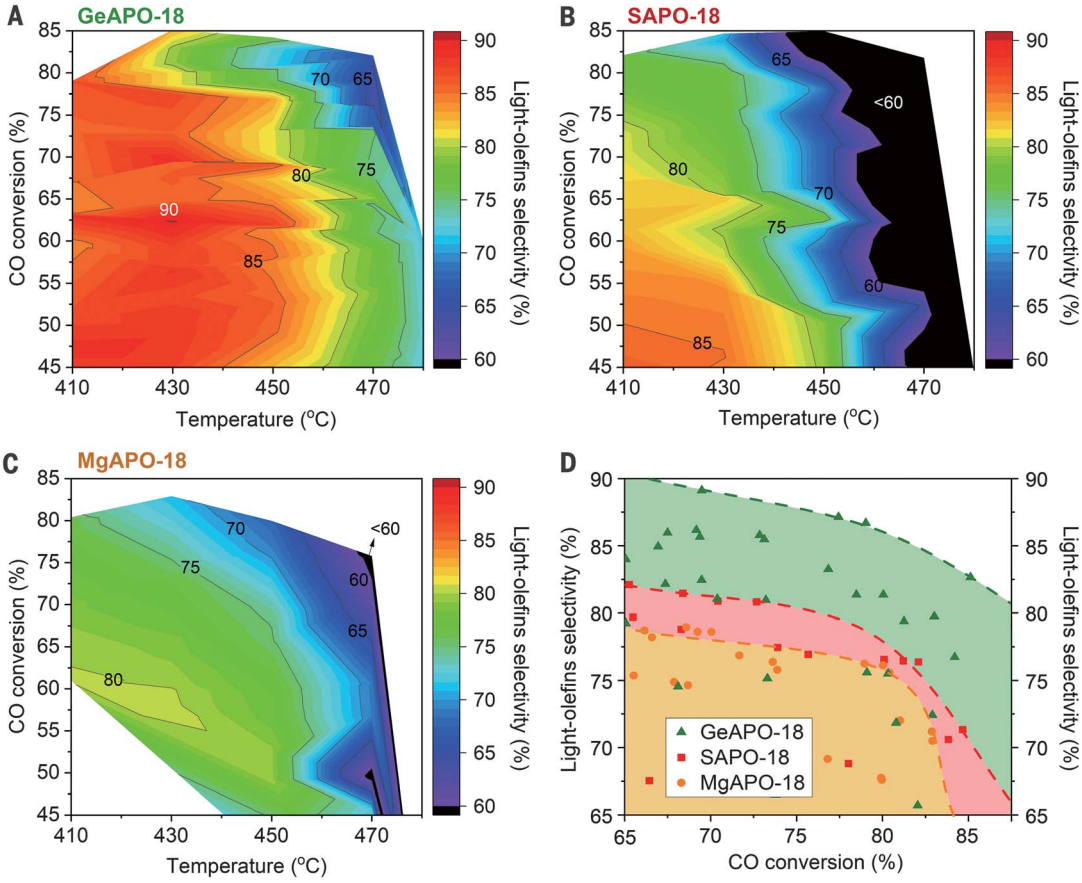

Fig. 3. Comparison of $ZnCrO_x$-MeAPO-18 in syngas conversion. Contour plots of catalytic performance. (**A**) GeAPO-18 with Ge/Al = 0.012 to 0.027. (**B**) SAPO-18 with Si/Al = 0.011 to 0.029. (**C**) MgAPO-18 with Mg/P = 0.019 to 0.029. (**D**) Selectivity of light olefins versus CO conversion, with the dashed lines being guides for the eye. Reaction condition: H_2/CO = 2.5, 410° to 480°C, 6 MPa, 1500 to 6000 ml/(g·hour).

by changing their acidity properties (varying Si/Al and Mg/P ratios) or the reaction conditions, but it can be breached by GeAPO-18.

Mechanistic studies

We compared GeAPO-$18_{0.025}$, SAPO-$18_{0.016}$, and MgAPO-$18_{0.029}$ to understand the mechanism underlying the high yield of olefins over the $ZnCrO_x$–GeAPO-18 catalysts because all three catalysts have a similar density of the medium-strength acid sites (table S4) as well as comparable diffusion efficiency (fig. S18). The NH_3-TPD profiles in fig. S11 show that the desorption corresponding to the medium-strength acid sites peaks at 235°C for GeAPO-$18_{0.025}$, which is 50°C lower than that of SAPO-$18_{0.016}$. In comparison, MgAPO-18 shows a broad high-temperature desorption feature (between 300° and 413°C). The desorption temperatures reveal that the strength of the acidity decreased in the sequence of MgAPO-18 > SAPO-18 > GeAPO-18. These results were consistent with the experimentally measured differential adsorption heat of NH_3 (table S7) and NH_3 binding energy on different Brønsted acid sites calculated with density functional theory (DFT) (table S8 and figs. S8 and S19), which were, respectively, 143 kJ/mol and −1.24 eV for GeAPO-$18_{0.025}$, 156 kJ/mol, and −1.40 eV for SAPO-$18_{0.016}$, and 193 kJ/mol and −1.71 eV for MgAPO-$18_{0.029}$.

Because the light-olefins yield improved with decreasing strength of the zeotype acidity, we examined the effect of the acidity on the adsorption and activation of H_2 and olefins by using ethylene as a probe molecule (table S9 and figs. S8 and S20). The calculated mean ethylene adsorption energy was 0.56 ± 0.05 eV on the Ge–OH–Al Brønsted acid sites (Fig. 4A), which was noticeably weaker than that on Si–OH–Al and Mg–OH–P sites. This order correlated well with the NH_3 binding energy trend, even considering the variation of the energies on different T-sites of each zeotype (Fig. 4A), and was further confirmed with the ethylene-TPD experiments (Fig. 4B). The H-D exchange experiments revealed a weaker H_2 activation activity on GeAPO-$18_{0.025}$ than that on SAPO-$18_{0.016}$ and MgAPO-$18_{0.029}$ (Fig. 4C) (*31*).

Both the weaker ethylene adsorption and H_2 activation over GeAPO-18 retard the secondary reactions of ethylene hydrogenation to ethane and its oligomerization to higher hydrocarbons C_{3+} (*18*). This is further demonstrated by ethylene conversion in the presence of hydrogen between 400° and 460°C over MeAPO-18 (Fig. 4D and fig. S21). GeAPO-18 exhibited lower activity for ethylene hydrogenation and oligomerization than those of the other two zeotypes. Although the presence of CO could significantly suppress the secondary reactions of olefins, GeAPO-18 still exhibited the weakest activity among the three zeotypes (fig. S22). The above results demonstrated that the Ge–OH–Al site can modulate the relative kinetics of C–C coupling of ketene to olefins and the subsequent over-hydrogenation and oligomerization of olefins and hence results in high selectivity for light olefins. The weaker oligomerization activity of Ge–OH–Al sites, as another advantage, led to a higher selectivity to more valuable ethylene and propylene compared with that of the optimized SAPO-18 under the same conditions (tables S10 and S11), which is of economic importance for industrial application. Therefore, CO conversion is improved by increasing the density of Ge–OH–Al sites and optimization of reaction conditions without degrading the light-olefins selectivity (Fig. 2A and fig. S23). An even higher activity can be expected if more Ge–OH–Al Brønsted acid sites could be generated as soon as a suitable preparative technique for enhanced heterometal substitution into zeotype frameworks becomes available (fig. S23).

Discussion

This study demonstrates that the key to breaking the activity and selectivity trade-off in CO hydrogenation to olefins lies in the disentanglement of the catalytically active sites for

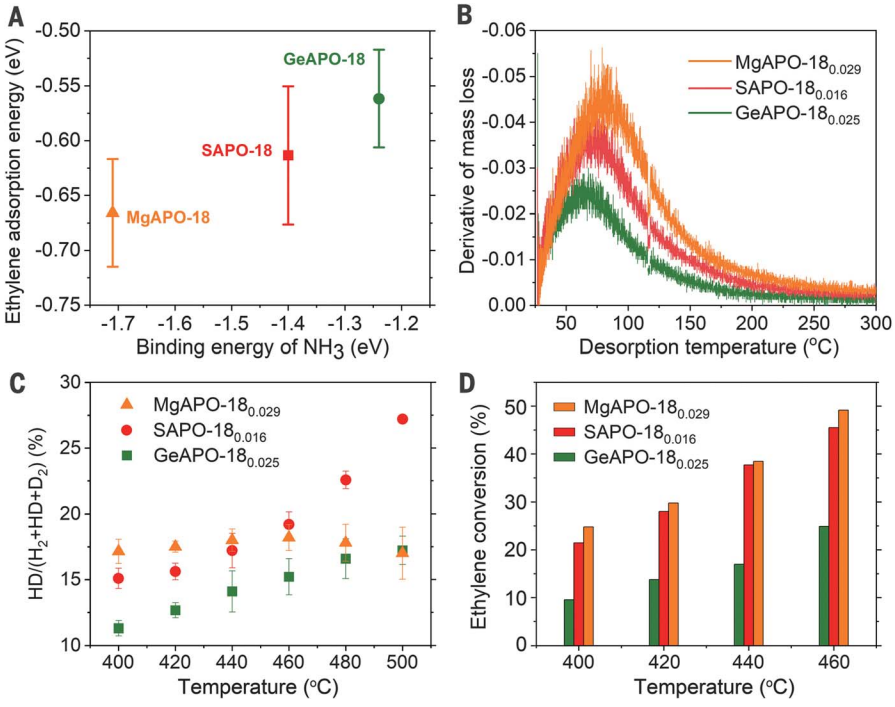

Fig. 4. Acidic strength of GeAPO-18 and its effects on the catalytic performance in comparison with SAPO-18 and MgAPO-18. (**A**) Calculated mean adsorption energy of ethylene versus the binding energy of NH_3. The error bars indicating the variation of adsorption energy between different T-sites of zeotypes (tables S8 and S9). (**B**) Ethylene-TPD measured by the derivative of the mass loss detected with intelligent gravimetric analysis. (**C**) H-D exchange activity represented by the relative $HD/(H_2+HD+D_2)$ concentration. (**D**) Ethylene hydrogenation at 400° to 460°C, 4 MPa, 200 ml/min, feed 1.2% C_2H_4-66.6% H_2-32.2% Ar.

the target and side reactions. It demonstrates that incorporation of Ge-substituted AlPO-18 provides an effective strategy within the OXZEO catalyst concept. Its weaker Ge–OH–Al Brønsted acid sites are largely inactive for the secondary reactions of hydrogenation and oligomerization of olefins, and increasing the density of Brønsted acid sites does not strengthen the acidity. Therefore, one can create more active sites to catalyze the conversion of ketene intermediates to light olefins and thus shift the thermodynamically limiting step of syngas conversion to ketene. As a result, 85% CO conversion and 83% light-olefins selectivity can be simultaneously obtained, resulting in an unprecedented light-olefins yield of 48% under optimized conditions. Furthermore, metal substitution constitutes a general strategy to mediate the strength and density of Brønsted acid sites in zeotype frameworks, which will enable the optimization of catalysts not only for CO but also CO_2 hydrogenation to value-added chemicals.

REFERENCES AND NOTES

1. U. Zavyalova, M. Holena, R. Schlögl, M. Baerns, *ChemCatChem* **3**, 1935–1947 (2011).
2. C. Zhan *et al.*, *J. Am. Chem. Soc.* **142**, 14134–14141 (2020).
3. Q. Q. Guan *et al.*, *Nat. Catal.* **4**, 840–849 (2021).
4. J. T. Hu *et al.*, *Nat. Catal.* **4**, 242–250 (2021).
5. C. Wang *et al.*, *J. Am. Chem. Soc.* **144**, 16855–16865 (2022).
6. F. Jiao *et al.*, *Science* **351**, 1065–1068 (2016).
7. X. Pan, F. Jiao, D. Miao, X. Bao, *Chem. Rev.* **121**, 6588–6609 (2021).
8. H. M. Torres Galvis *et al.*, *Science* **335**, 835–838 (2012).
9. Y. Xu *et al.*, *Science* **371**, 610–613 (2021).
10. C. Wang *et al.*, *Nat. Nanotechnol.* **17**, 714–720 (2022).
11. L. Zhong *et al.*, *Nature* **538**, 84–87 (2016).
12. J. Xie *et al.*, *Nat. Commun.* **10**, 167 (2019).
13. W. Fang *et al.*, *Science* **377**, 406–410 (2022).
14. K. Cheng *et al.*, *Angew. Chem. Int. Ed.* **55**, 4725–4728 (2016).
15. Y. Wang, *J. Energy Chem.* **25**, 169–170 (2016).
16. J. Su *et al.*, *Nat. Commun.* **10**, 1297 (2019).
17. P. Gao, L. Zhong, B. Han, M. He, Y. Sun, *Angew. Chem. Int. Ed.* **61**, e202210095 (2022).
18. G. Li *et al.*, *ACS Catal.* **10**, 12370–12375 (2020).
19. X. L. Liu *et al.*, *ACS Catal.* **10**, 8303–8314 (2020).
20. L. Tan *et al.*, *Chem. Sci.* **11**, 4097–4105 (2020).
21. N. Li *et al.*, *Nat. Commun.* **13**, 2742 (2022).
22. H. Wang *et al.*, *Natl. Sci. Rev.* **9**, nwac146 (2022).
23. P. Zhang *et al.*, *Ind. Eng. Chem. Res.* **60**, 13214–13222 (2021).
24. Y. Ding *et al.*, *ACS Catal.* **11**, 9729–9737 (2021).
25. Z. Z. Lai *et al.*, *ACS Catal.* **11**, 12977–12988 (2021).
26. J. Kanai *et al.*, *J. Catal.* **133**, 527–543 (1992).
27. S. Senger, L. Radom, *J. Am. Chem. Soc.* **122**, 2613–2620 (2000).
28. A. Vityuk *et al.*, *ACS Catal.* **9**, 839–847 (2019).
29. X. Liu *et al.*, *Chem. Sci.* **9**, 4708–4718 (2018).
30. H. M. Torres Galvis, K. P. de Jong, *ACS Catal.* **3**, 2130–2149 (2013).
31. H. H. Shin, S. McIntosh, *J. Mater. Chem. A* **1**, 7639–7647 (2013).

ACKNOWLEDGMENTS

We gratefully acknowledge Y. Li for his contribution in material synthesis. We thank beamline BL14W1 (Shanghai Synchrotron Radiation Facility) for the beam time and assistance with experiments. We thank X. Huang for discussion on XAS data analysis and H. Wang for discussion on Intelligent Gravimetric Analyzer data analysis. **Funding:** This work was supported by the Ministry of Science and Technology of China (2018YFA0704503), the National Natural Science Foundation of China (grants 91945302, 22272167, and 22002153), the Chinese Academy of Sciences (XDA21020400), the Youth Innovation Promotion Association of Chinese Academy of Sciences (2019184), and the Dalian Science and Technology Innovation Fund (2022RY02). **Author contributions:** F.J., G.L., C.X., Y.D., and J.L. performed the catalyst preparation. F.J., S.Q., and B.B. performed the catalytic reaction test. B.B., C.X., Z.J., W.L., T.P., and C.L. performed the characterization. Y.Y. and J.X. performed the DFT calculation. F.J., X.P., and X.B. designed the study, analyzed the data, and wrote the paper. **Competing interests:** A Chinese patent application (CN2018115750600) and six international patent applications (SA521421990; RU2021113024; ZA2021/02711; US17/286,903; IN202127019453; and EP19900221.3) through the Patent Cooperation Treaty (PCT) have been submitted by F.J., G.L., X.P., and X.B. **Data and materials availability:** All data are available in the manuscript and the supplementary materials.

SUPPLEMENTARY MATERIALS

science.org/doi/10.1126/science.adg2491
Materials and Methods
Supplementary Text
Figs. S1 to S23
Tables S1 to S12
References

Submitted 14 December 2022; accepted 17 April 2023
10.1126/science.adg2491

Disentangling the activity-selectivity trade-off in catalytic conversion of syngas to light olefins

Feng Jiao, Bing Bai, Gen Li, Xiulian Pan, Yihan Ye, Shengcheng Qu, Changqi Xu, Jianping Xiao, Zhenghao Jia, Wei Liu, Tao Peng, Yilun Ding, Cheng Liu, Jinjing Li, and Xinhe Bao

Science, **380** (6646), .
DOI: 10.1126/science.adg2491

Editor's summary

The production of light olefins from a mixture of hydrogen and carbon monoxide (syngas) over metal-oxide zeolite catalysts is complicated by competing side reactions. Jiao *et al*. show that the Brønsted acid sites created in the zeolite AlPO-18 by germanium substitution were highly active for carbon–carbon coupling of the intermediates to olefins but much weaker for the unwanted side reactions of hydrogenation and olefin oligomerization. A carbon monoxide conversion of 85%, along with a selectivity of for light olefins of 83%, led to an overall yield of almost 50%. —Phil Szuromi